frontiers | Frontiers in Energy Research

TYPE Original Research
PUBLISHED 26 September 2023
DOI 10.3389/fenrg.2023.1240473

OPEN ACCESS

EDITED BY
Olusegun David Samuel,
Federal University of Petroleum Resource Effurun, Nigeria

REVIEWED BY
Andrea Toscani,
University of Parma, Italy
Kenneth E. Okedu,
Melbourne Institute of Technology, Australia

*CORRESPONDENCE
Xiaoguang Kong,
kongxiaoguang@syuct.edu.cn

RECEIVED 15 June 2023
ACCEPTED 12 September 2023
PUBLISHED 26 September 2023

CITATION
Kong X, Zhang Y and Xu G (2023), Optimal design and control of permanent magnet assisted dual rotor motor.
Front. Energy Res. 11:1240473.
doi: 10.3389/fenrg.2023.1240473

Optimal design and control of permanent magnet assisted dual rotor motor

Xiaoguang Kong*, Yaowen Zhang and Gepeng Xu

School of Information Engineering, Shenyang University of Chemical Technology, Shenyang, China

As high-performance motors, permanent magnet motors are widely used in a wide range of applications. It has become a consensus to mine reluctance torque in permanent magnet motors. The combination of permanent magnet motors and reluctance motors to generate higher output torque is one of the hotspots in motor research. A dual-rotor motor can be formed by connecting a coaxial connector or a concentric end disk, which can make the motor generate higher torque. However, although the motor torque has been improved, the cogging torque still affects the output torque of the motor. This paper describes a method to reduce the cogging torque of the permanent magnet rotor of the permanent magnet-assisted double rotor motor. By analyzing the motor power equation, it is concluded that the pole arc coefficient, the thickness of the magnetic steel, the length of the air gap, and the slot width of the stator have four influences on the teeth. For the parameters of the slot torque, the upper and lower limits of the parameter value are obtained according to the size of the motor. A certain parameter is taken as a fixed value, and the remaining parameters are uniformly valued. Use parametric scanning to determine the optimal value range of the parameter, and use Maxwell for parameterization. Simulation and analysis show that the cogging torque of the motor is reduced by 90% and the torque ripple is reduced by 50%. In order to simplify the motor control system, this paper designs a fuzzy controller based on granular functions, and the fuzzy rules of the fuzzy controller are to perform feature sampling and fit the response function, eliminating fuzzification and defuzzification, improving the response speed of fuzzy control, and simplifying the control system.

KEYWORDS

dual rotor, permanent magnet synchronous motor, cogging torque, parameter scan, granular function

1 Introduction

The advantages of permanent synchronous motors include their small size, light size, minimal loss, outstanding performance, and wide range of applications (Wang and Leng, 2018). They are widely used for various occasions and equipment. However, due to the high price and limited supply of rare earth magnets, the development of high-performance motors without rare earths has gradually attracted great attention. Reducing the use of permanent magnets in permanent magnet motors and using synchronous reluctance motors without permanent magnets are feasible alternatives. The synchronous reluctance motor has a reliable mechanical design, a low cost, and a multi-barrier construction that can efficiently

enhance the output torque, but its applicability is also constrained by its drawbacks of poor torque density and low factor (Hofmann and Sanders, 2000).

The two ideal properties of a motor are high torque density and high efficiency (Agbo et al., 2021). Due to its high torque density and high space efficiency, the double-rotor motor has always been a research focus for scientists. In recent years, in order to further improve the motor efficiency and torque density, scientists from different countries have developed various types of double rotor motors, such as double rotor permanent magnet motors with different pole topologies (NS) (Qu and Lipo, 2003) and double rotor disc motors with modified stator core yoke (Liu and Li, 2022), steel sheets instead of part of the permanent magnets reduce the Manufacturing cost of the double rotor axial flux motor (Diao et al., 2023), and there is also a concentric switched double-rotor reluctance motor that integrates two rotors and two stators into a compact and robust structure (Aravind et al., 2011; Al-Ani, 2021), and a switched double-rotor reluctance motor with magnetic isolation ring (Shirzad, 2023), and yokeless double-rotor mutual coupling switched reluctance motor (Fu et al., 2023); magnetic field modulation brushless double-rotor machine (Bai et al., 2015), double-rotor in-wheel motor with multiple operating modes (Li et al., 2023) Permanent magnet reluctance dual rotor motor (Li et al., 2017), and so on. In general, it is mainly divided into permanent magnet double rotor motors and reluctance double rotor motors. In this paper, combining the advantages of a permanent magnet motor and a reluctance motor, a permanent magnet-assisted dual-rotor motor is proposed.

In order to achieve the goals of high torque density and wide constant-speed operating range, a permanent magnet assisted dual-rotor motor is proposed in this paper, which adopts a dual-rotor radial flux configuration, combining the synchronous reluctance rotor and the permanent magnet rotor with rare earth permanent magnets to form a single motor entity, the design can control reluctance torque and permanent magnet torque more flexibly, since the cogging torque determines the torque ripple, and the torque ripple affects the quality of the output torque, therefore the goal of the permanent magnet synchronous motorization of the outer rotor is to reduce the cogging torque, according to the definition of the cogging torque, determine the parameters that affect the cogging torque, such as the pole arc coefficient, considering that the parameters have little influence on each other, the parameter sweep method can be used. The range of parameter optimization is given according to the size constraints of the motor, and the cogging torque of the permanent magnet rotor is optimized. Through the simulation analysis of the optimized motor model, the effectiveness of this optimization scheme is verified. Finally, the permanent magnet-assisted dual-rotor motor designed in this paper has the characteristics of a magnetic isolation ring. The motor is split into internal and external parts for control. The internal and external motor control systems share a speed loop and are equipped with hysteresis controllers, respectively. The internal and external motors use torque ratios for current distribution and introduce granular functions to improve the constant fuzzy speed loop, which simplifies the control system and improves the rapidity and robustness of motor response.

2 Motor preliminary design

2.1 Motor topology

The outer rotor of a permanent magnet assisted dual rotor motor is a surface-mounted permanent rotor, which shares several characteristics with permanent magnet dual rotor motors. The distinction is that the permanent magnet synchronous motor and the synchronous reluctance motor are integrated into a single motor, and the synchronous reluctance rotor is used to replace the internal permanent magnet rotor (Yunyun et al., 2012). The two rotors share a shaft and rotate at the same mechanical speed. The stator winding adopts the ring winding method, and the magnetomotive force direction of the stator winding of the outer motor is opposite that of the stator winding of the inner motor. In order to achieve magnetic insulation between the inner stator and the outer stator, a magnetic insulator used as a barrier ring is used in the middle of the stator yoke. The insulator is made of brass. Figure 1 is a three-dimensional diagram of the motor. The parameters of the motor are shown in Table 1.

In order to ensure that the motor outputs ideal torque, the internal synchronous reluctance rotor should be properly designed. The typical number of rotor poles of a synchronous reluctance motor is four, but this requires the external surface-mounted permanent magnet rotor to also maintain a four-pole topology. This design method will cause the external permanent magnet rotor yoke to become thicker, and with added weight comes reduced performance. The external surface-mounted permanent magnet rotor is more suitable for the application of multi-rotor pole topology to reduce the thickness of the yoke and the weight of the motor, but this type of topology is not the best design for synchronous reluctance motors because, because of the multi-pole structure, the pole speed of the magnetization inductor of the synchronous reluctance rotor will decrease, and the performance

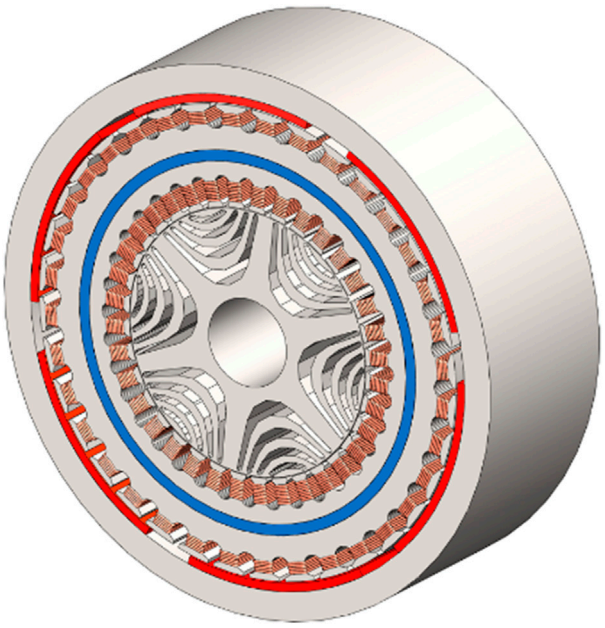

FIGURE 1
3D model of motor.

TABLE 1 Main parameters of the motor.

Parameter	Data	
	Internal motor	External motor
Rotor pole number	6	6
Number of stator slots	36	36
Stator radius/mm	48.65	63.95
Outer radius of rotor/mm	36	74.65
Inner radius of rotor/mm	12	66.65
Air gap length/mm	0.35	0.5
Length of iron core/mm	70	70
Power rating/kw	1	2
Speed/rpm	1,600	1,600

of the synchronous reluctance rotor will also decrease under the condition of a high pole number. Therefore, the number of rotor poles selected for this type of motor is six, and the number of poles of the inner and outer rotors is the same, so as to balance the low number of magnetic poles of the synchronous reluctance rotor and the high number of magnetic poles of the surface-mounted permanent magnet rotor.

The design of the synchronous reluctance rotor flux barrier focuses on the number and position of each flux barrier layer. Generally, for the inner rotor synchronous reluctance motor, the torque ripple decreases with the increase of the number of flux barriers, but due to the limitations of the manufacturing process, the rotor flux barriers are generally set to 4 layers in the design of the synchronous reluctance motor (Jurca and Martis, 2017), so the number of rotor magnetic barriers in this paper is also set to 4 layers.

Different windings, cogging slots, permanent magnet arrangements, and reluctance rotor magnetic barrier shapes of permanent magnet-assisted dual-rotor motors have various topological structures. The permanent magnet rotor can not only be installed on the surface but also be buried in the ground, and the shape of the magnetic barrier of the reluctance rotor can also be LAL, ARC, segmented rectangle, etc. Figure 2 shows the permanent magnet rotor and a few examples of magnetic choke rotors.

2.2 Motor power equation

2.2.1 External permanent magnet motor

The rated output power of the motor is the product of the number of phases, voltage, and current of the motor. There must be conversion efficiency in power conversion, and the stator waveform of the motor is a rectangular wave rather than a sine wave in most cases. Therefore, it is necessary to multiply the motor efficiency coefficient η and the shape coefficient k_p, Therefore, after ignoring the loss caused by the external stator winding impedance and leakage inductance, the output power of the external permanent magnet motor P_{spm} can be expressed as:

$$P_{spm} = \eta m k_p E_{pk} I_{pk} \tag{1}$$

Among them, η is the motor efficiency; m is the number of phases; k_p is the power form factor; E_{pk} is the peak value of the back electromotive force of the single-phase winding; I_{pk} is the peak value of the stator phase current. Since the stator current vector is aligned with the back EMF vector, the d-axis current is 0, and the value of k_p can be set to 0.5.

The peak value of the back electromotive force of the external permanent magnet motor can be expressed as the product of the peak value of the air gap flux density, the effective length of the winding, and the speed at which the winding cuts the magnetic induction line, $E = BLV$. Among them, the peak value of the air gap magnetic field can be expressed by $B_{gl.p}$, and the effective length of the winding can be expressed as the product of the number of turns N_t of each phase winding, the winding coefficient K_w and the axial length L_e, since the length of the air gap is very short, for an external rotor motor, the linear velocity of a point on the outer diameter of the stator can be used to represent the linear velocity of a certain point in the air gap, so the linear velocity of a certain point in the air gap can be calculated by the formula $v = 2\pi rn$ express, for an external rotor motor, the formula should be expressed as $v = 2\pi\frac{D_{os}}{2}(\frac{f_e}{p})$, so the peak value of the back electromotive force of the external permanent magnet rotor E_{pk} can be expressed as:

$$E_{pk} = B_{gl.p} * K_w N_t L_e * 2\pi \frac{D_{os}}{2}\left(\frac{f_e}{p}\right) = \pi K_w N_t B_{gl.p}\left(\frac{f_e}{p}\right) D_{os} L_e \tag{2}$$

Among them, K_w is the winding coefficient; N_t is the number of winding turns per phase; $B_{gl.p}$ is the peak value of the surface-mounted permanent magnet rotor side air gap flux density; f_e is the power supply frequency; p is the number of pole pairs; D_{os} is the permanent The outer diameter of the stator of the magneto; L_e is the axial length of the motor core, v is the linear velocity of a certain point in the air gap, r is the radius of the motor, and n is the speed of the motor.

Use the electrical load value $A_{sp.rms}$ on the rotor side to represent the peak value of the stator phase current I_{pk}, $A_{sp.rms}D_{os}\pi$ represents the current effective value of the electrical load, $\frac{A_{sp.rms}D_{os}\pi}{m}$ represents the effective value of current that each phase needs to provide to the load, $\frac{A_{sp.rms}D_{os}\pi}{mN_t}$ represents the effective value of current that each turn of wire needs to provide to the load, and the current peak value needs to be multiplied by the coefficient $\sqrt{2}$, so the peak value of the stator phase current can be expressed as $\sqrt{2}\ \frac{A_{sp.rms}D_{os}\pi}{mN_t}$, after adjusting the parameter position, peak current I_{pk} can be obtained:

$$I_{pk} = \frac{\sqrt{2}D_{os}\pi}{mN_t} A_{sp.rms} \tag{3}$$

Substituting parameters in Eqs 2, 3 into Eq. 1, the output power of the motor can be expressed as:

$$P_{spm} = \frac{\sqrt{2}\pi^2}{2} K_w \eta \left(\frac{f_e}{p}\right) B_{gl.p} A_{sp.rms} D_{os}^2 L_e \tag{4}$$

2.2.2 Internal reluctance motor

The stator winding must supply the d-axis and q-axis current components to generate the reluctance torque, so in the expression, the formula needs to be multiplied by an included angle coefficient $\cos\gamma$. The constraint equation of the synchronous reluctance rotor can be compared to the constraint equation of the permanent magnet synchronous motor. The difference is that the

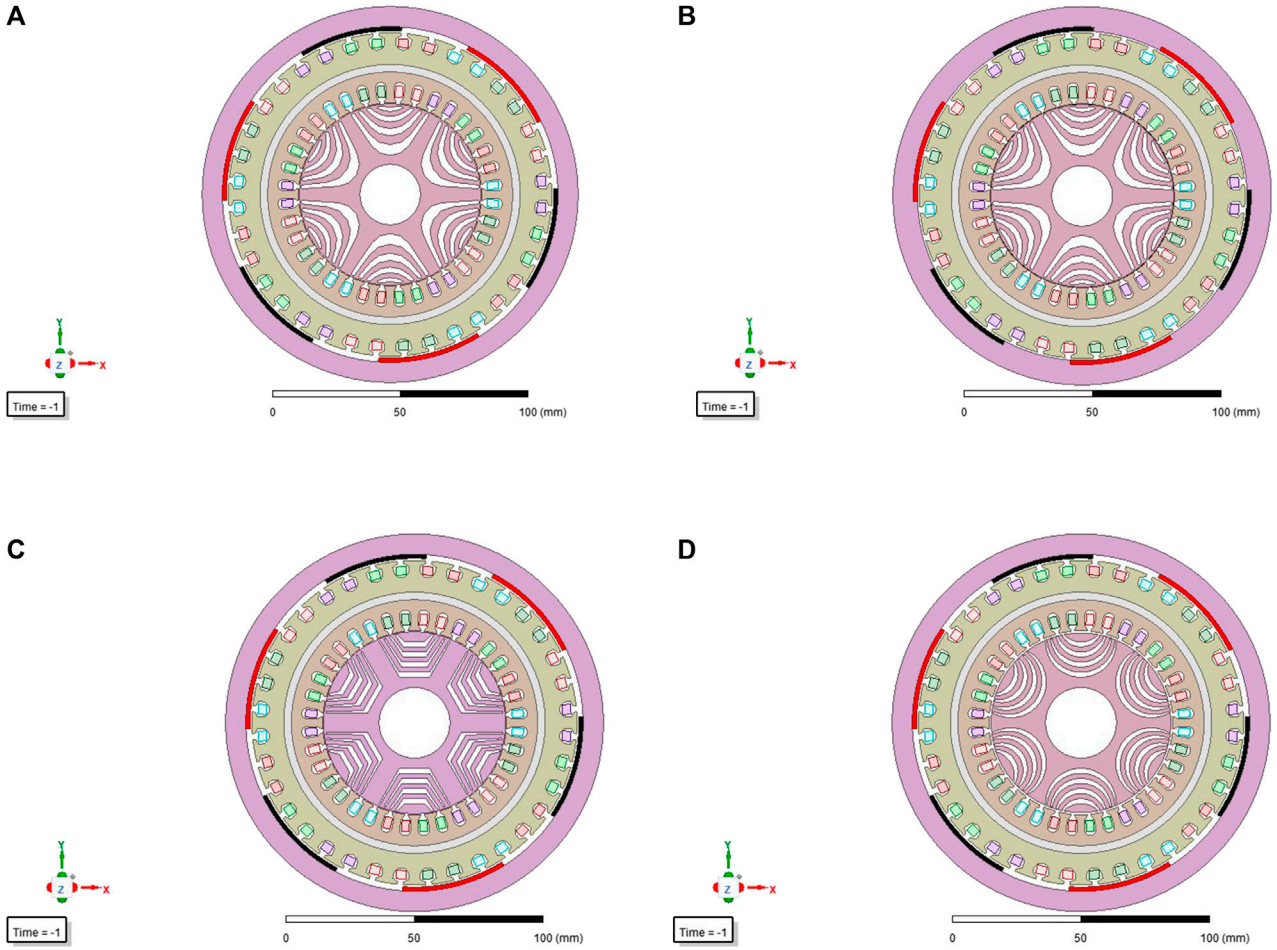

FIGURE 2
Other types of permanent magnet assisted reluctance dual-rotor motor topology: **(A)** Hyperbolic magnetic barrier, **(B)** Plug-in permanent magnet, **(C)** Segmented magnetic barrier, **(D)** ARC barrier.

TABLE 2 Optimize the parameter range.

Parameter	The lower limit	The upper limit
Polar arc coefficient	0.6	0.76
Stator slot width/mm	1.2	3
Permanent magnet thickness/mm	1	2.6
Air gap length/mm	0.2	1.6

synchronous reluctance rotor does not have a permanent magnet that generates back electromotive force. As a result, the synchronous reluctance rotor's output power P_{syr} can be stated as:

$$P_{syr} = \frac{\sqrt{2}\pi^2}{2} K_w \eta \left(\frac{f_e}{p}\right) \cos\gamma B_{g1.R} A_{sR.rms} D_{is}^2 L_e \tag{5}$$

Among them, $\cos\gamma$ is the power factor of the inner rotor motor, γ is the angle between the q-axis component and the stator current; $B_{g1.R}$ is the peak value of the air gap magnetic flux density of the synchronous reluctance rotor side; $A_{sR.rms}$ is the electrical load value on the rotor side of the synchronous reluctance; D_{is} is the inner diameter of the stator of the synchronous reluctance motor.

2.2.3 Double rotor motor

By combining the constraint equations of the external permanent magnet motor and the internal reluctance motor, the complete constraint equation of the dual-rotor motor can be derived, the output power P_{total} is expressed as:

$$P_{total} = \frac{\sqrt{2}\pi^2}{2} K_w \eta \left(\frac{f_e}{p}\right) L_e \left[B_{g1.R} A_{sR.rms} D_{is}^2 \cos\gamma + B_{g1.p} A_{sp.rms} D_{os}^2\right] \tag{6}$$

Since the inner and outer motor stator windings of the motor are connected in series, the winding currents are equal, so it can be obtained:

$$\frac{A_{sp.rms} D_{os} \pi}{m N_t} = \frac{A_{sR.rms} D_{is} \pi}{m N_t} \tag{7}$$

A simple transformation can be obtained

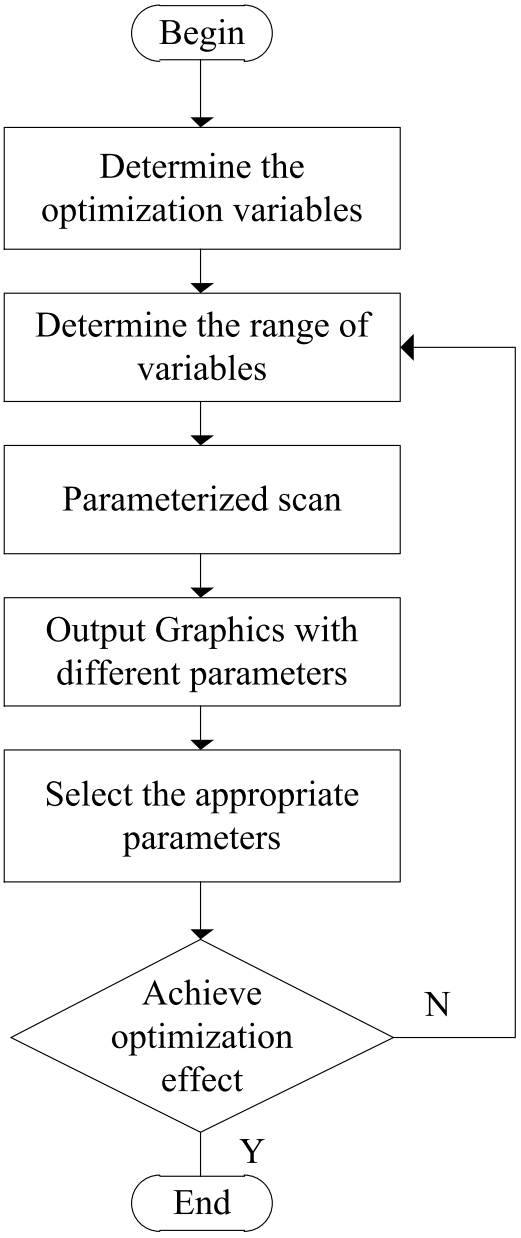

FIGURE 3
Flow chart of cogging torque optimization scheme.

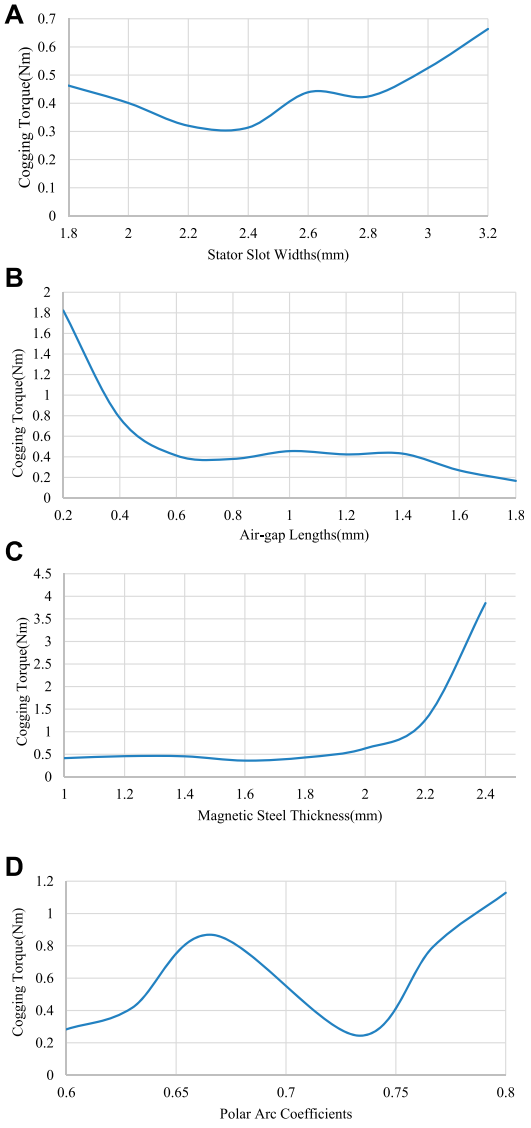

FIGURE 4
The maximum value of cogging torque when each parameter changes: **(A)** Maximum cogging torque at different stator slot widths, **(B)** Maximum cogging torque at different air-gap lengths, **(C)** Maximum cogging torque at different magnet thicknesses, **(D)** Maximum cogging torque at different polar arc coefficients.

$$A_{sp.rms}D_{os} = A_{sR.rms}D_{is} \tag{8}$$

The relationship between the load on the inner rotor side and the outer rotor side can be expressed by the ratio of the inner diameter of the inner motor to the outer diameter of the outer motor:

$$A_{sR.rms} = \frac{D_{is}}{D_{os}}A_{sR.rms} \tag{9}$$

Putting Formula (9) into Formula (6), after simplification, motor total power P_{total} can be expressed as:

$$P_{total} = \frac{\sqrt{2}\pi^2}{2}K_w\eta\left(\frac{f_e}{p}\right)\left[B_{g1.R}\cos\gamma + B_{g1.P}\frac{D_{os}}{D_{is}}\right]A_{sR.rms}D_{is}^2L_e \tag{10}$$

3 Cogging torque optimization

3.1 Cogging torque and optimization method

A major contributor to torque ripple in permanent magnet motors is the cogging torque (Wang et al., 2011). In order to reduce the influence of the cogging torque on the surface-mount permanent magnet motor, Patel (2023) recommended slotting to reduce the gear toque by 48.78%. Rashid and Mohammed (2023) proposed a sawtooth moment mitigation method based on the radial slits of the pole pieces. Won et al. (2023) used neural network prediction to achieve the purpose of reducing cogging torque. Wang et al. (2023) adopted the method of combining in-phase unit (IPU) grouping and slotting angle

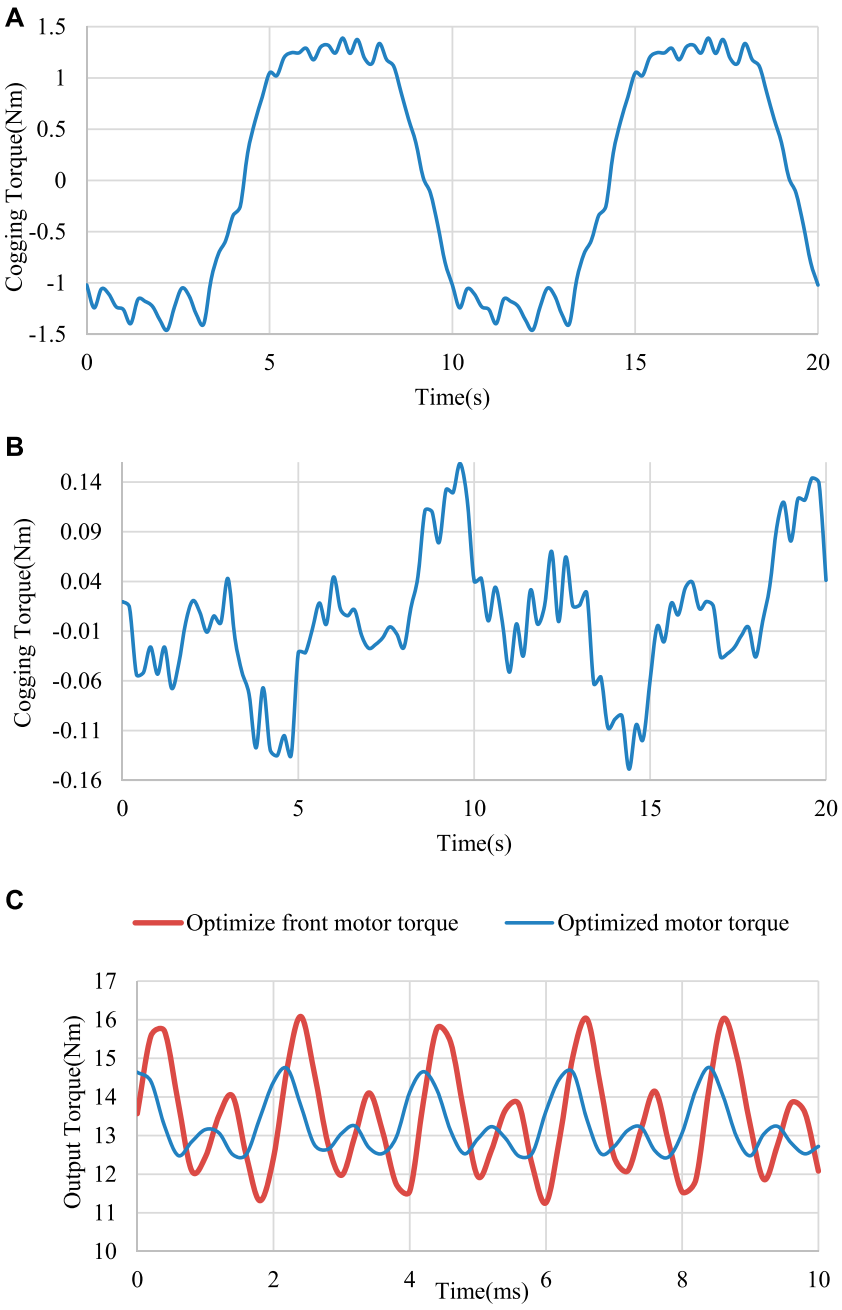

FIGURE 5
Waveform comparison before and after optimization: **(A)** Cogging torque waveform before optimization, **(B)** Cogging torque waveform after optimization, **(C)** Output torque waveform before and after optimization.

offset so that the main harmonic component of the sawtooth torque is cancelled to achieve the purpose of reducing the cogging torque.

This paper chooses to determine the factors affecting cogging torque from the definition of cogging torque. Cogging torque T_{cog} is defined as the negative derivative of the magnetic energy w with respect to the position angle α when de-energized. The expression can be derived as follows:

$$T_{cog}(\alpha) = \frac{\pi z L_e}{4u_0}\left(R_2^2 - R_1^2\right)\sum_{n=1}^{\infty} nG_n B_{rn}\, sin(nz\alpha) \tag{11}$$

In the formula, R_1 is outside armature diameter of external motor, R_2 is stator inner diameter of external motor, z is number of stator slots, α is the relative position angle between the stator and rotor, u_0 is vacuum permeability.

B_{rn} is the Fourier coefficient of the residual flux density squared along the circumference of permanent magnets, and the formula is as follows:

$$B_{rn} = \frac{2}{n\pi} B_r^2 \sin n\alpha_p \pi \tag{12}$$

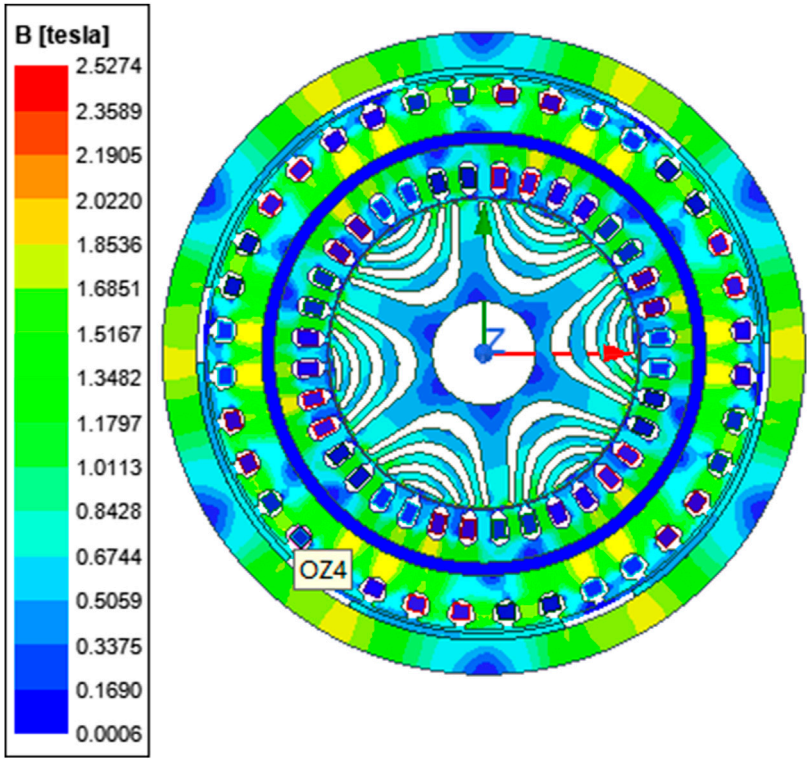

FIGURE 6
Motor magnetic field density map.

In the formula, B_r is the residual flux density in a permanent magnet, α_p is polar arc coefficient of permanent magnetic pole.

G_n is the Fourier coefficient of the square relative permeability of the air-gap and the formula is as follows:

$$G_n = \sum_{n=1}^{\infty} \frac{2}{n\pi} \left(\frac{h_m}{h_m + \delta} \right)^2 \sin\left(n\pi - \frac{nz\theta_s}{2} \right) \tag{13}$$

In the formula, δ is air gap length, h_m is the thickness of the permanent magnet along the magnetization direction, θ_s is the corresponding radian value of the width of the stator groove.

3.2 Determine optimization variables and parameter ranges

It can be seen from the above formula that the slot opening angle width, magnetic steel angle width, magnetic steel thickness, and air gap length all have a great influence on the cogging torque. Therefore, these four parameters are selected as the cogging torque optimization parameters in this paper to study their effect on cogging torque. Table 2 lists the optimized variable parameter ranges.

3.3 Parameter optimization

In order to explore the law of cogging torque weakening caused by different design variables, each design variable is parameterized in the optimization process, and one parameter is selected as a variable. The upper and lower limits are given as shown in Table 2. Other parameters are constants; after obtaining the waveforms of the cogging torque in various situations, select the maximum value to draw the trend of the cogging torque changing with the parameters, and select the optimal parameters for simulation verification in Maxwell. If the optimal effect meets expectations, the optimization is complete. If the effect is not as expected, it is necessary to change the upper and lower limits of the parameters or to optimize the parameters. The specific optimization scheme flow chart is shown in Figure 3. As we can see in Figure 4, the optimal values of the four parameters can be easily found according to the graph.

3.4 Optimization results

During the cogging torque parameterization, different degrees of attenuation can be demonstrated by using different methods and changing the parameter range. It can be seen from Figure 4 that when the pole arc coefficient is between 0.72 and 0.74 and the thickness of the magnetic steel is between 1.6 mm and 1.8 mm, the calculated cogging torque is relatively lower. Considering that increasing the air gap will reduce the output torque of the motor, the length of the air gap should be kept between 0.6 mm and 1 mm. The cogging torque waveform before and after adjustment is shown in Figure 5. The cogging torque is reduced from 1.5 Nm to 0.15 Nm, and the optimized output torque waveform is more stable, the torque ripple is lower, and the optimization effect is more obvious.

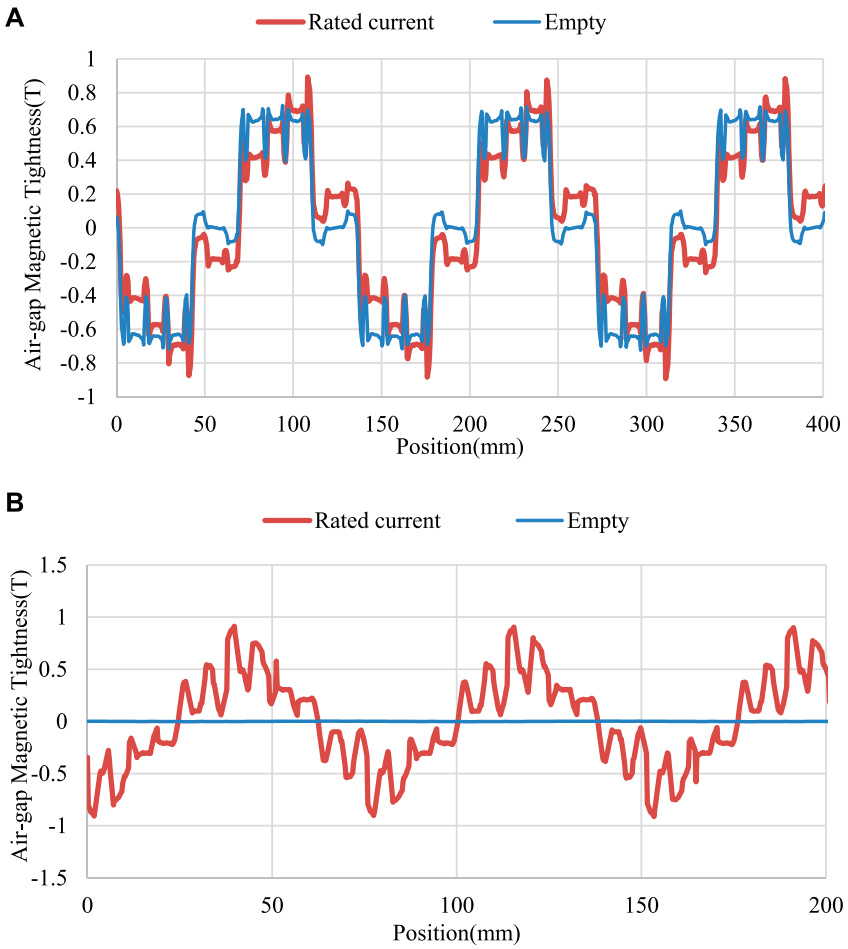

FIGURE 7
Air gap magnetic: **(A)** Outer motor air gap flux density and **(B)** Inner motor air gap flux density.

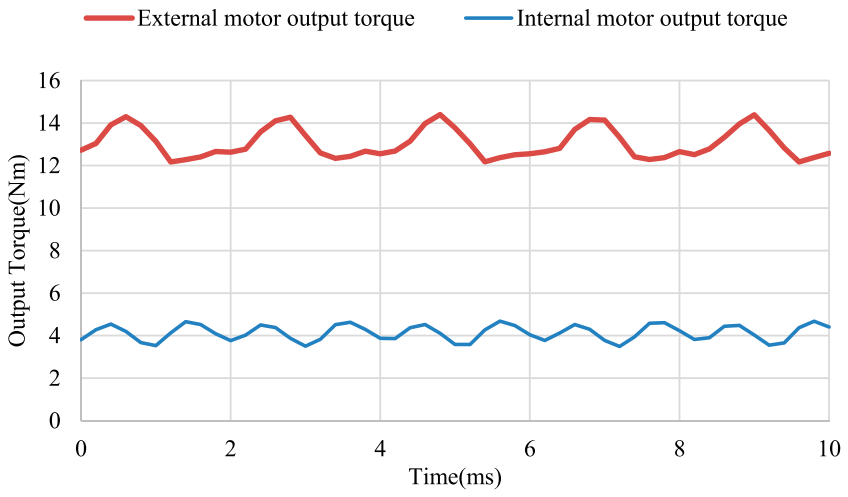

FIGURE 8
Output torque waveform of internal and external motors.

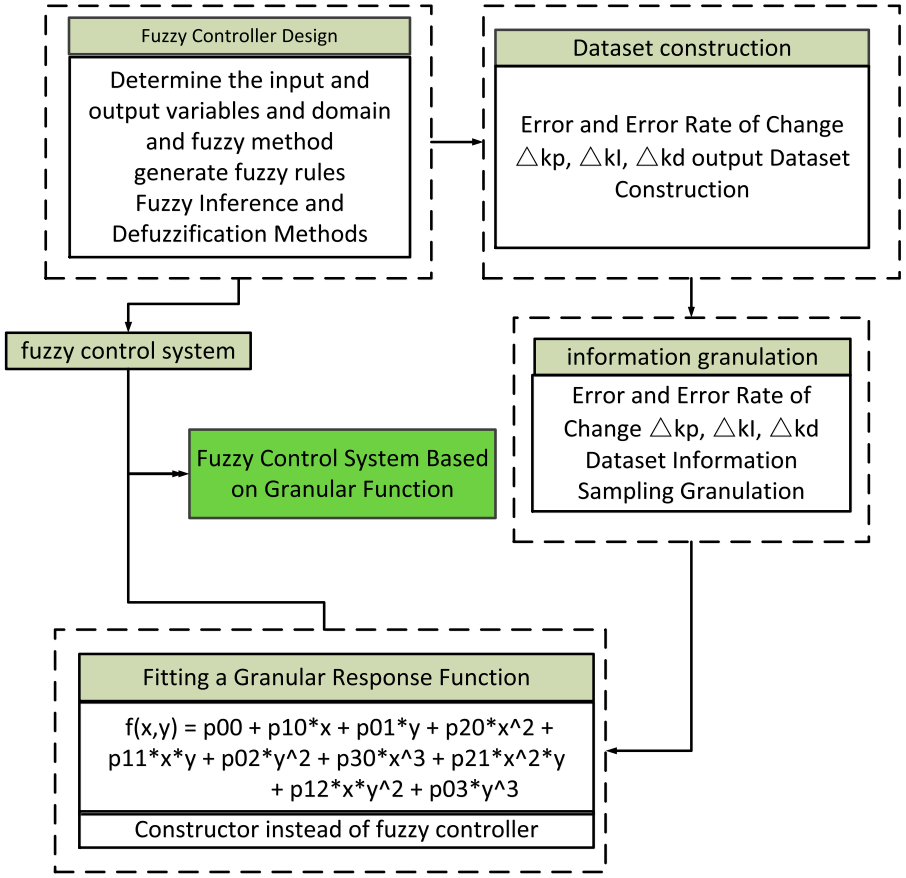

FIGURE 9
Construction process of granular function optimization fuzzy controller.

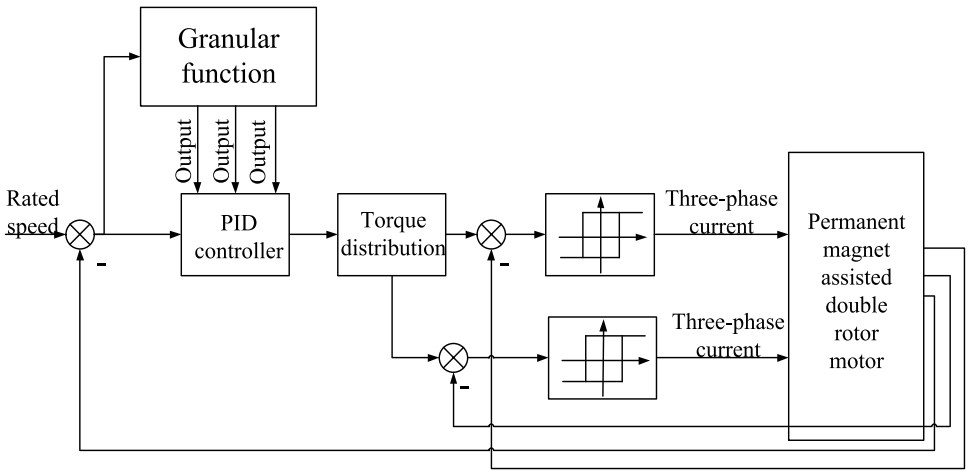

FIGURE 10
Control system block diagram.

4 Electromagnetic characteristic analysis

4.1 Magnetic flux density

After the optimization is completed, use the finite element software Maxwell to establish a two-dimensional model of the motor, set the rated current on the inner and outer stator windings, and obtain the magnetic flux density cloud diagram of the permanent magnet assisted dual-rotor motor with load through finite element simulation. As shown in Figure 6, the maximum value of the magnetic flux density appears at the position of the inner and outer stator yoke, which is about 1.8T, which does not exceed the design limit of 2T and meets the motor operation specification.

4.2 Air gap magnetic density

The air-gap magnetic field density is an important indicator of motor design. Figure 7 is the air-gap flux density curve of the internal and external motors under no-load and rated current. The amplitude of the air-gap flux density reflects the magnetic field strength and torque density of the motor, it can be seen that the waveform is closer to a sine wave. From the comparison of the two curves, we can see that the air gap flux density curve of the inner motor is more reasonable than the sinusoidal distribution of the outer motor, indicating that the inner motor can meet the requirements of torque output and power density. The peak values of the air gap magnetic density of the outer motor and the inner motor are 0.8T and 1 T, respectively, which generally meet the design requirements.

4.3 Output torque

Since the motor has a double-air-gap structure, its total output torque is the sum of the output torques of the inner and outer motors, and the torque output waveforms of the inner and outer motors are shown in Figure 8. According to the output torque results, the output torque of the inner rotor synchronous reluctance motor is about 4 Nm, and the torque ripple is about 28.8%. The output torque of the outer rotor permanent magnet synchronous motor is about 13 Nm, and the torque ripple is about 17.1%, which verifies the effectiveness of the optimized design, and the quality of the motor output torque has been significantly improved.

5 Design of control system for dual rotor motor

5.1 Motor mathematical model

The dual-rotor motor is composed of inner rotor, outer rotor, permanent magnet, magnetic isolation ring and other parts. It has the characteristics of strong coupling and nonlinearity. For the convenience of analysis, the assumptions are as follows: 1) Neglect eddy current and hysteresis loss; 2) Excitation current There is no response time; 3) The stator windings are star-connected, and the stator windings are connected in parallel. According to the above assumptions, it can be obtained that the dual-rotor motor can be split into a permanent magnet synchronous motor and a synchronous reluctance motor, and after transformation by clark and park the voltage equation of the motor under the dq axis.

$$\begin{bmatrix} u_{d1} \\ u_{q1} \end{bmatrix} = \begin{bmatrix} \cos\theta_1 & \cos\left(\theta_1 - \frac{2\pi}{3}\right) & \cos\left(\theta_1 - \frac{4\pi}{3}\right) \\ -\sin\theta_1 & -\sin\left(\theta_1 - \frac{2\pi}{3}\right) & -\sin\left(\theta_1 - \frac{4\pi}{3}\right) \end{bmatrix} \begin{bmatrix} U_{A1} \\ U_{B1} \\ U_{C1} \end{bmatrix} \quad (14)$$

$$\begin{bmatrix} u_{d2} \\ u_{q2} \end{bmatrix} = \begin{bmatrix} \cos\theta_2 & \cos\left(\theta_2 - \frac{2\pi}{3}\right) & \cos\left(\theta_2 - \frac{4\pi}{3}\right) \\ -\sin\theta_2 & -\sin\left(\theta_2 - \frac{2\pi}{3}\right) & -\sin\left(\theta_2 - \frac{4\pi}{3}\right) \end{bmatrix} \begin{bmatrix} U_{A2} \\ U_{B2} \\ U_{C2} \end{bmatrix} \quad (15)$$

Since the double-rotor motor is divided into two parts, the inner rotor and the outer rotor, the electromagnetic torque of the motor is expressed as the permanent magnet torque of the outer motor and the reluctance torque of the inner motor, and the sum of the inner and outer torques is the total electromagnetic torque of the motor.

$$T_e = T_{e1} + T_{e2} = \frac{3}{2} p_1 \left(L_{d1} - L_{q1}\right) i_{d1} i_{q1} + \frac{3}{2} p_2 i_{q2} \psi_f \quad (16)$$

$$T_e - T_L = J\frac{d\omega}{dt} + B\omega \quad (17)$$

In these formulas, p_x is the logarithm of the motor poles, U_{Ax} U_{Bx} U_{Cx} is the motor stator three-phase current, i_{dx} i_{qx} is current of dq axial, u_{dx} u_{qx} is voltage of dq axial, θ_x is angle from abc axial to dq axial, T_{ex} is the electromagnetic torque of a motor, T_L is a load torque, B is the damping coefficient, ω is the mechanical speed of a motor, J is the moment of inertia of the motor, ψ_f is the permanent magnet linkage of a motor. x equals to 1 is the reluctance part of the motor, x equals to 2 is the permanent magnet portion of the motor.

5.2 Vector control

Vector control is based on the control idea of a DC motor, converts the three-phase current into excitation current and torque current, and realizes indirect control of the motor by changing the magnitude of the excitation current and torque current, that is, by controlling the axis current of the motor to achieve the purpose of controlling the motor. At present, the commonly used vector control methods of permanent magnet synchronous motors include $i_d = 0$ control, $\cos\varphi = 1$ control, maximum torque-current ratio control and flux weakening control; vector control methods of synchronous reluctance motor include maximum torque-to-current ratio control, maximum power factor control, maximum torque change rate control, and so on. The external motor of the double-rotor motor is a surface-mounted permanent magnet synchronous motor, and the $i_d = 0$ control is equivalent to the maximum torque-to-current ratio control, therefore, the inner and outer motors of the dual-rotor motor in this paper are controlled by the maximum torque-current ratio, which simplifies the control system.

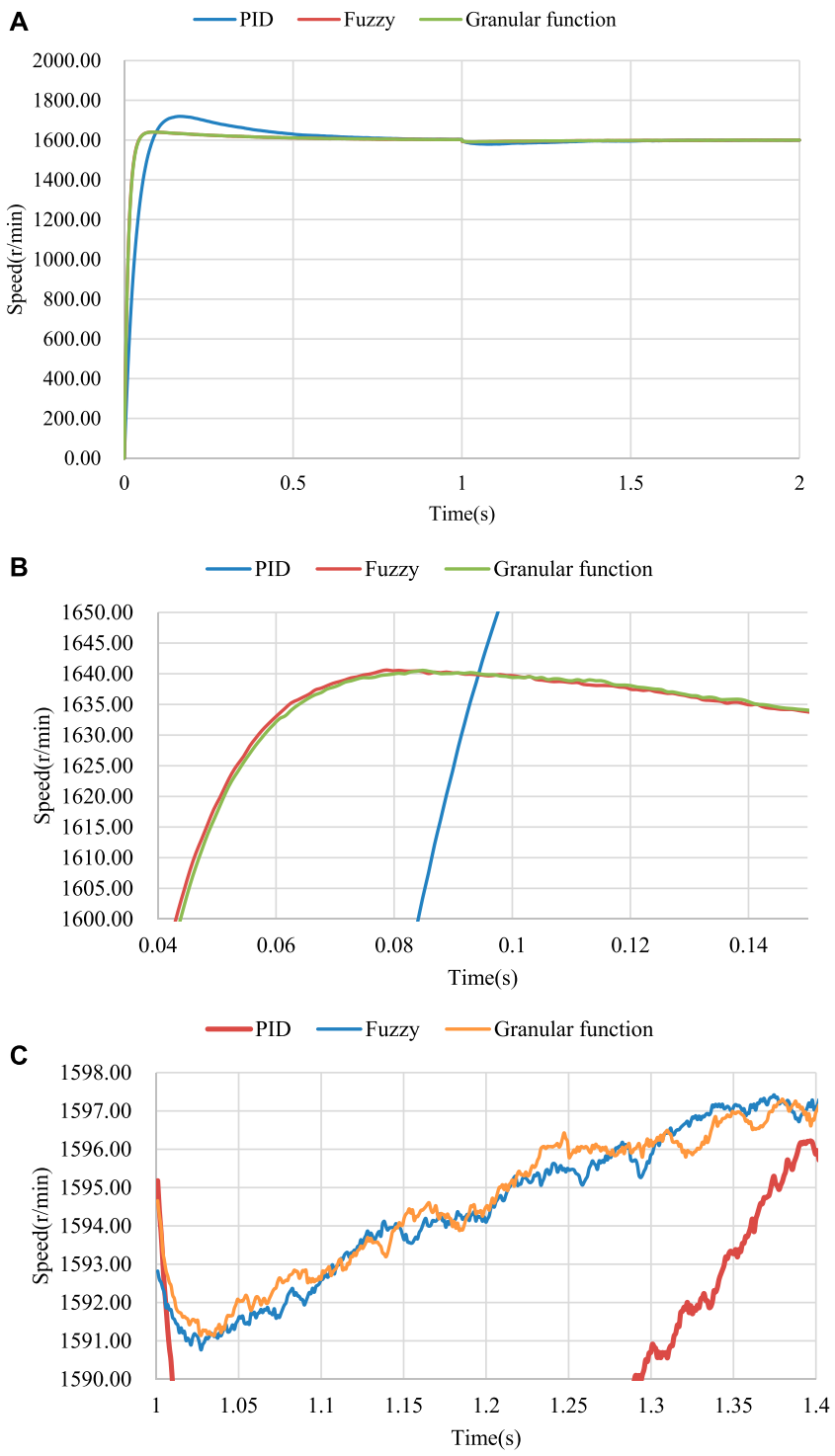

FIGURE 11
Motor output waveform: **(A)** The output waveforms of different control modes, **(B)** Partial enlarged view of the speed increase process. **(C)** Partial enlarged view of the speed drop process after.

5.3 Torque distribution

Due to the existence of the magnetic isolation ring, the dual-rotor motor can be equivalent to a surface-mounted permanent magnet synchronous motor and a synchronous reluctance motor. Conventional control requires two sets of controllers that interact with each other. In order to solve this problem, torque distribution is introduced. Torque distribution is used to fix the ratio of the output torque of the internal and external motors, distribute the torque current of the internal and external motors, and simplify the control system.

5.4 Controller design

5.4.1 Current controller design

The current controller in this design adopts the mode of hysteresis control, also called bang-bang control, which has the characteristics of real-time control, fast reaction, and strong robustness. The implementation method is to change the switching state of the inverter by comparing the given current value with the detected current value, and then output the actual current in the shape of a sawtooth wave. Although there are certain errors, this current control method is simple and easy to implement and does not rely on motor parameters.

5.4.2 Speed controller design

The speed control of this design adopts the granular function instead of the fuzzy controller. The granular function is based on the theory of granular computing. Granular computing (GrC) is usually defined in an informal way as a general computing theory that can be used effectively. To build an efficient computational model for complex applications with large amounts of data, information, and knowledge (Bargiela and Pedrycz, 2008), the granular function shifts from a machine-centered approach to a human-centered approach. It is one of the trends in granular computing research (Yao, 2010), and fuzzy set theory is an application of granular computing (Zarandi Baghini et al., 2023). The construction of granular functions in fuzzy control is divided into steps such as information sampling, information granulation, and fitting. Using granular functions instead of fuzzy controllers can save steps such as fuzzification and defuzzification. The construction process of a granular computing fuzzy controller is shown in Figure 9.

5.5 System simulation and analysis

5.5.1 Control system block diagram

According to the description of the fuzzy control optimized by the above granular function, a dual-rotor motor control system frame can be built as shown in Figure 10. The control system is composed of a traditional PID controller, a granular function optimization module, a torque distribution module, a current hysteresis controller, and a motor body.

5.5.2 Simulation result analysis

As shown in Figure 11, the highest speed for fuzzy control and granular function control is about 1,640 r/min, and after changing the load, fuzzy control and granular function control motors drop to 1,591 r/min. It can be concluded that the granular function is comparable to the fuzzy control in terms of control performance, but the granular function removes the complicated fuzzification and defuzzification processes, only needs one response function, and the simulation time is less than one-tenth of the fuzzy control.

6 Conclusion

This paper aims to address the problem that the cogging torque of a dual-rotor motor connected by concentric end disks affects the motor's output torque. By deriving the motor power equation constraints, the fixed-value scanning method is used for optimization analysis. After optimization, the motor cogging torque was reduced from 1.5 Nm to 0.15 Nm, a reduction of 90%; the external rotor torque ripple was reduced by 50%; the torque output waveform was improved; and the optimized electromagnetic performance was verified. Finally, in order to simplify the motor control system, this paper uses granular functions to improve the fuzzy controller, performs feature sampling on fuzzy rules, and uses response functions to replace the fuzzy controller, omitting the fuzzification and defuzzification links. Simulation shows that after granular function optimization, the response speed of the system is significantly improved.

Data availability statement

The original contributions presented in the study are included in the article/Supplementary Materials, further inquiries can be directed to the corresponding author.

Author contributions

YZ and GX wrote and typed the manuscript, and XK provided writing guidance, checking and correction.

Funding

This work is supported in part by the National Natural Science Foundation of China under grant 51877139 and the Basic Scientific Research Project of Liaoning Provincial Department of Education of China under grant LJKMZ20220778.

Conflict of interest

The authors declare that the research was conducted in the absence of any commercial or financial relationships that could be construed as a potential conflict of interest.

Publisher's note

Supplementary material

The Supplementary Material for this article can be found online at: https://www.frontiersin.org/articles/10.3389/fenrg.2023.1240473/full#supplementary-material

References

Agbo, S., Samuel, O. D., Amosun, S. T., Oyejide, O. J., Fayomi, O. S. I., Bamisaye, O. S., et al. (2021). Development of a solar energy-powered surface water pump. *IOP Publ.* 1107 (1), 012002. doi:10.1088/1757-899X/1107/1/012002

Al-Ani, M. (2021). Multi-physics design and analyses of dual rotor synchronous reluctance machine. *eTransportation* 8, 100113. doi:10.1016/j.etran.2021.100113

Aravind, C. V., Norhisam, M., Aris, I., Marhaban, M. H., Ahmad, D., and Nirei, M. (2011). "Double-rotor switched reluctance machine (DRSRM): fundamentals and magnetic circuit analysis," in 2011 IEEE Student Conference on Research and Development (IEEE), 294–299.

Bai, J., Zheng, P., Cheng, L., Zhang, S., Liu, J., and Liu, Z. (2015). A new magnetic-field-modulated brushless double-rotor machine. *IEEE Trans. Magnetics* 51 (11), 1–4. doi:10.1109/tmag.2015.2445917

Bargiela, A., and Pedrycz, W. (2008). Toward a theory of granular computing for human-centered information processing. *IEEE Trans. Fuzzy Syst.* 16 (2), 320–330. doi:10.1109/tfuzz.2007.905912

Diao, C., Zhao, W., Ding, H., and Wang, X. (2023). *Design and analysis of low-cost double rotor axial flux permanent magnet synchronous motor*.

Fu, D., Lv, Z., Si, H., Liu, Y., and Wu, X. (2023). *Analysis and comparison of novel yokeless double rotor mutually coupled switched reluctance motor*.

Hofmann, H., and Sanders, S. R. (2000). High-speed synchronous reluctance machine with minimized rotor losses. *IEEE Trans. Industry Appl.* 36 (2), 531–539. doi:10.1109/28.833771

Jurca, F., and Martis, C. (2017). "Analysis of outer rotor synchronous reluctance motor for low-speed applications[C]," in 2017 19th International Conference on Electrical Drives and Power Electronics (EDPE), Dubrovnik, Croatia, 04-06 October 2017 (IEEE), 242–247.

Li, J., Wang, J., Liu, J., and Ren, C. (2023). Coordinated control strategy for drive mode switching of double rotor in-wheel motor based on MPC and control allocation. *World Electr. Veh. J.* 14 (5), 132. doi:10.3390/wevj14050132

Li, Y., Bobba, D., and Sarlioglu, B. (2017). Design and optimization of a novel dual-rotor hybrid PM machine for traction application. *IEEE Trans. Industrial Electron.* 65 (2), 1762–1771. doi:10.1109/tie.2017.2739686

Liu, Y., and Li, J. (2022). Research on concentrated winding counter-rotating double rotor disk motor. *Mech. Des. Manuf.* (03), 110–113. doi:10.19356/j.cnki.1001-3997.20211115.003

Patel, A. N. (2023). *Slot opening displacement technique for cogging torque reduction of axial flux brushless DC motor for electric two-wheeler application*.

Qu, R., and Lipo, T. A. (2003). Dual-rotor, radial-flux, toroidally wound, permanent-magnet machines. *IEEE Trans. industry Appl.* 39 (6), 1665–1673. doi:10.1109/tia.2003.818968

Rashid, M. K., and Mohammed, A. M. (2023). A reduction method of cogging torque for magnetic gears. *Iran. J. Electr. Electron. Eng.* 19 (2), 2752. doi:10.22068/IJEEE.19.2.2752

Shirzad, E. (2023). *Calculation of flux density in air-gap for reluctance motor with two ports (Double-Stator, double-rotor) by fourier series*.

Wang, D., Wang, X., Qiao, D., Pei, Y., and Jung, S. Y. (2011). Reducing cogging torque in surface-mounted permanent-magnet motors by nonuniformly distributed teeth method. *IEEE Trans. Magnetics* 47 (9), 2231–2239. doi:10.1109/tmag.2011.2144612

Wang, H., and Leng, J. (2018). "Summary on development of permanent magnet synchronous motor," in 2018 Chinese Control And Decision Conference (CCDC) (IEEE), 689–693.

Wang, L., Lu, S., Chen, Y., and Wang, S. (2023). An in-phase unit slot-opening shift method for cogging torque reduction in interior permanent magnet machine. *Mathematics* 11 (7), 1735. doi:10.3390/math11071735

Won, Y. J., Kim, J. H., Park, S. H., Lee, J. H., An, S. M., Kim, D. Y., et al. (2023). Transfer learning-based design method for cogging torque reduction in PMSM with step-skew considering 3-D leakage flux. *IEEE Trans. Magnetics*, 1. doi:10.1109/tmag.2023.3294601

Yao, J. (2010). Novel developments in granular computing: applications for advanced human reasoning and soft computation: applications for advanced human reasoning and soft computation. *IGI Glob*.

Yunyun, C., Li, Q., Xiaoyong, Z., Hua, W., and Wang, Z. (2012). Electromagnetic performance analysis of double-rotor stator permanent magnet motor for hybrid electric vehicle. *IEEE Trans. Magnetics* 48 (11), 4204–4207. doi:10.1109/tmag.2012.2206374

Zarandi Baghini, A., Babaei, H., Tabatabaei Mirhosseini, R., and Torkzadeh Tabrizi, L. (2023). New approach based on fuzzy hypergraphs in granular computing (an application to the urban vulnerability assessment). *Int. J. Nonlinear Analysis Appl.* doi:10.21203/rs.3.rs-1167172/v1